# A fluorescence LIDAR sensor for hyper-spectral time-resolved remote sensing and mapping

**Lorenzo Palombi, Daniele Alderighi, Giovanna Cecchi, Valentina Raimondi, Guido Toci, and David Lognoli***

*Institute for Applied Physics "Nello Carrara" - National Research Council of Italy, Via Madonna del Piano, 10, I50019 Sesto Fiorentino (FI), Italy*

**d.lognoli@ifac.cnr.it*

**Abstract:** In this work we present a LIDAR sensor devised for the acquisition of time resolved laser induced fluorescence spectra. The gating time for the acquisition of the fluorescence spectra can be sequentially delayed in order to achieve fluorescence data that are resolved both in the spectral and temporal domains. The sensor can provide sub-nanometric spectral resolution and nanosecond time resolution. The sensor has also imaging capabilities by means of a computer-controlled motorized steering mirror featuring a biaxial angular scanning with 200 μradiant angular resolution. The measurement can be repeated for each point of a geometric grid in order to collect a hyper-spectral time-resolved map of an extended target.



**OCIS codes:** (280.3640) Lidar; (300.2530) Fluorescence, laser-induced; (300.6500) Spectroscopy, time-resolved.

## References and links

1. R. M. Measures, *Laser Remote Sensing: Fundamentals and Applications* (Wiley, 1984).
2. B. Valeur and M. N. Berberan-Santos, *Molecular Fluorescence*, Second Edi (Wiley-VCH, 2012), pp. 1–569.
3. P. Weibring, H. Edner, and S. Svanberg, "Versatile mobile LiDAR system for environmental monitoring," Appl. Opt. **42**(18), 3583–3594 (2003).
4. C. W. Wright, F. E. Hoge, R. N. Swift, J. K. Yungel, and C. R. Schirtzinger, "Next-Generation NASA airborne oceanographic LiDAR system," Appl. Opt. **40**(3), 336–342 (2001).
5. L. Pantani, G. Ballerini, G. Cecchi, H. Edner, D. Lognoli, T. Johansson, V. Raimondi, S. Svanberg, P. Tiano, L. Tomaselli, and P. Weibring, "Experiments on stony monument monitoring by laser-induced fluorescence," J. Cult. Herit. **1**, S345–S348 (2000).
6. V. Raimondi, G. Cecchi, D. Lognoli, L. Palombi, and G. Ballerini, "The fluorescence LIDAR technique for the cultural heritage," in *Handbook on the Use of Lasers in Conservation and Conservation Science*, M. Schreiner and M. Strilic, eds. (COST Office, 2008), Vol. 7, pp. 3.6.1–3.6.18.
7. C. E. Brown and M. F. M. Fingas, "Review of the development of laser fluorosensors for oil spill application," Mar. Pollut. Bull. **47**(9-12), 477–484 (2003).
8. I. Mochi, M. Bazzani, G. Cecchi, C. Cucci, D. Lognoli, L. Pantani, V. Raimondi, D. Tirelli, G. Valmori, M. Abbate, and S. Fontani, "High-resolution lidar fluorescence spectra for the characterization of phytoplankton," in *International Symposium on Remote Sensing*, M. Owe, C. R. Bostater, Jr., H. Fujisada, K. P. Schaefer, A. Kohnle, S. B. Serpico, M. Ehlers, F. Posa, J. D. Gonglewski, O. Lado-Bordowsky, J. B. Lurie, R. Santoleri, G. D'Urso, L. Toulios, M. L. Aten, A. Comeron, R. H. Picard, and K. Weber, eds. (2003), pp. 117–126.
9. S. R. Rogers, T. Webster, W. Livingstone, and N. J. O'Driscoll, "Airborne Laser-Induced Fluorescence (LIF) Light Detection and Ranging (LiDAR) for the quantification of dissolved organic matter concentration in natural waters," Estuaries Coasts **35**(4), 959–975 (2012).
10. S. Svanberg, "Fluorescence lidar monitoring of vegetation status," Phys. Scr. T **T58**, 79–85 (1995).
11. V. Raimondi, G. Cecchi, L. Pantani, and R. Chiari, "Fluorescence lidar monitoring of historic buildings," Appl. Opt. **37**(6), 1089–1098 (1998).
12. L. Pantani, G. Cecchi, D. Lognoli, I. Mochi, V. Raimondi, D. Tirelli, M. Trambusti, G. Valmori, P. K. A. Weibring, H. Edner, T. Johansson, and S. Svanberg, "Lithotypes characterization with a fluorescence lidar imaging system using a multi-wavelength excitation source," in *Remote Sensing for Environmental Monitoring, GIS Applications, and Geology II*, M. Ehlers, ed. (2003), pp. 151–159.
13. G. Ballerini, S. Bracci, L. Pantani, and P. Tiano, "Lidar remote sensing of stone cultural heritage: detection of protective treatments," Opt. Engineer. **40**(8), 1579 (2001).

#184545 - $15.00 USD Received 14 Feb 2013; revised 10 May 2013; accepted 10 May 2013; published 13 Jun 2013

14. D. Lognoli, G. Lamenti, L. Pantani, D. Tirelli, P. Tiano, and L. Tomaselli, "Detection and Characterization of Biodeteriogens on Stone Cultural Heritage by Fluorescence Lidar," Appl. Opt. **41**(9), 1780–1787 (2002).
15. V. Raimondi, G. Cecchi, D. Lognoli, L. Palombi, R. Grönlund, A. Johansson, S. Svanberg, K. Barup, and J. Hällström, "The fluorescence lidar technique for the remote sensing of photoautotrophic biodeteriogens in the outdoor cultural heritage: A decade of in situ experiments," Int. Biodeter. Biodegr. **63**(7), 823–835 (2009).
16. F. Castagnoli, G. Cecchi, L. Pantani, I. Pippi, B. Radicati, and P. Mazzinghi, "A Fluorescence LIDAR For Land And Sea Remote Sensing," in *Laser Radar Technology and Applications I*, J. M. Cruickshank and R. C. Harney, eds. (1986), pp. 212–216.
17. M. U. Piracha, D. Nguyen, D. Mandridis, T. Yilmaz, I. Ozdur, S. Ozharar, and P. J. Delfyett, "Range resolved lidar for long distance ranging with sub-millimeter resolution," Opt. Express **18**(7), 7184–7189 (2010).
18. D. Lognoli, G. Cecchi, I. Mochi, L. Pantani, V. Raimondi, R. Chiari, T. Johansson, P. Weibring, H. Edner, and S. Svanberg, "Fluorescence lidar imaging of the cathedral and baptistery of Parma," Appl. Phys. B **76**(4), 457–465 (2003).
19. K. Ohm, R. Reuter, M. Stolze, and R. Willkomm, "Shipboard oceanographic fluorescence lidar development and evaluation based on measurements in Antarctic waters," EARSeL Advances in Remote Sensing **5**, 105–113 (1997).
20. R. Barbini, F. Colao, R. Fantoni, C. Frassanito, A. Palucci, and S. Ribezzo, "Range resolved lidar fluorosensor for marine investigation," in *EARSeL-SIG-Workshop LIDAR* (2000), pp. 175–184.
21. R. M. Measures, W. R. Houston, and D. G. Stephenson, "Laser induced fluorescent decay spectra - a new form of environmental signature," Opt. Engineer. **13**, 494–501 (1974).
22. E. Hegazi, A. Hamdan, and J. Mastromarino, "Remote fingerprinting of crude oil using time-resolved fluorescence spectra," Arab. J. Sci. Eng. **30**, 3–12 (2005).
23. P. Camagni, G. Colombo, C. Koechler, A. Pedrini, N. Omenetto, and G. Rossi, "Diagnostics of oil pollution by laser-induced fluorescence," IEEE T. Geosci. Remote **26**(1), 22–26 (1988).
24. L. Palombi, D. Lognoli, V. Raimondi, G. Cecchi, J. Hällström, K. Barup, C. Conti, R. Grönlund, A. Johansson, and S. Svanberg, "Hyperspectral fluorescence lidar imaging at the Colosseum, Rome: Elucidating past conservation interventions," Opt. Express **16**(10), 6794–6808 (2008).
25. J. Hällström, K. Barup, R. Grönlund, A. Johansson, S. Svanberg, L. Palombi, D. Lognoli, V. Raimondi, G. Cecchi, and C. Conti, "Documentation of soiled and biodeteriorated facades: A case study on the Coliseum, Rome, using hyperspectral imaging fluorescence lidars," J. Cult. Herit. **10**(1), 106–115 (2009).
26. F. Colao, R. Fantoni, L. Fiorani, A. Palucci, and I. Gomoiu, "Compact scanning lidar fluorosensor for investigations of biodegradation on ancient painted surfaces," J. Optoelectron. Adv. Mater. **7**, 3197 (2005).
27. U. Rascher, G. Agati, L. Alonso, G. Cecchi, S. Champagne, R. Colombo, A. Damm, F. Daumard, E. de Miguel, G. Fernandez, B. Franch, J. Franke, C. Gerbig, B. Gioli, J. A. Gómez, Y. Goulas, L. Guanter, Ó. Gutiérrez-de-la-Cámara, K. Hamdi, P. Hostert, M. Jiménez, M. Kosvancova, D. Lognoli, M. Meroni, F. Miglietta, A. Moersch, J. Moreno, I. Moya, B. Neininger, A. Okujeni, A. Ounis, L. Palombi, V. Raimondi, A. Schickling, J. A. Sobrino, M. Stellmes, G. Toci, P. Toscano, T. Udelhoven, S. van der Linden, and A. Zaldei, "CEFLES2: the remote sensing component to quantify photosynthetic efficiency from the leaf to the region by measuring sun-induced fluorescence in the oxygen absorption bands," Biogeosciences **6**(7), 1181–1198 (2009).
28. V. Raimondi, L. Palombi, D. Lognoli, G. Cecchi, and L. Masotti, "Design and development of a new high speed performance fluorescence imaging lidar for the diagnostic of indoor and outdoor cultural heritage," in *Lasers in the Conservation of Artworks*, M. Castillejo, P. Moreno, M. Oujja, R. Radvan, and J. Ruiz, eds. (CRC Press 2008, 2008), pp. 163–168.
29. A. C. Anigrisani, D. Calcaterra, P. Cappelletti, A. Colella, M. Parente, R. Prikryl, and M. De Gennaro, "Geological features, technological characterization and weathering phenomena of the Miocene Bryozoan and Lithothamnion limestones (central-southern Italy)," Ital. J. Geosci. **130**, 75–92 (2011).
30. J. R. Bezouska, J. Wang, and O. C. Mullins, "Origin of Limestone Fluorescence," Appl. Spectrosc. **52**(12), 1606–1613 (1998).
31. R. C. M. Sales and D. D. Brunelli, "Luminescence spectroscopy applied to a study of the curing process of diglycidyl-ether of bisphenol-A (DGEBA)," Mater. Res. **8**(3), 299–304 (2005).
32. J. C. Song and C. S. P. Sung, "Fluorescence studies of diaminodiphenyl sulfone curing agent for epoxy cure characterization," Macromolecules **26**(18), 4818–4824 (1993).
33. W. Koechner, "Solid-State Laser Engineering," Springer New York **1**, 490 (2006).
34. C. De Boor, *A Practical Guide to Splines* (Springer-Verlag, 1978), Vol. 27, p. 325.

## 1. Introduction

The excitation of a remote target by short laser pulses and the detection of the elastically and/or inelastically backscattered light is a widely used technique of investigation of the optical and electronic properties of the target and it is usually referred to as LIDAR (LIght Detection And Ranging) technique. Both the spectral and temporal characteristics of the light emitted by the target provide important information about the target nature and the phenomena occurring as a consequence of laser pulse excitation [1,2].

#184545 - $15.00 USD Received 14 Feb 2013; revised 10 May 2013; accepted 10 May 2013; published 13 Jun 2013

A huge variety of detectable targets have been studied by means of fluorescence LIDAR sensors mainly in environmental [3,4] and cultural heritage [5,6] fields. In environmental studies the applications have mainly been focused on oil spills detection and characterization [7], on the study of phytoplankton [8] and dissolved organic matter [9] in natural waters and on vegetation photosynthetic activity and health monitoring [10]. In the field of cultural heritage main investigated issues include the detection and characterization of different stones, mortars and other masonry materials [11,12], of protective treatments [13], of biodeteriogens and the analysis of the effects of biocide treatments [14,15].

The fluorescence LIDAR sensors have been mainly developed to acquire the return signal either using spectral resolution (and time integration) [16] or using temporal resolution but spectral integration over relatively broad bands [17]. As a consequence also the data processing methods have been focused either on the detailed examination of time-integrated, highly spectrally resolved data [18] or on the study of the temporal evolution of fluorescence signal in few spectral windows, in particular for the study of volume targets [19,20] or fluorescence decay times [21]. Few attempts of detecting time and wavelength resolved spectra of the emitted fluorescence are reported in the literature. Hegazi et al. [22] performed the acquisition of signal sequentially in the temporal domain using a scanning monochromator and a single photomultiplier with a gated integrator. Camagni et al. [23] used a gated multichannel sensor to perform the sequential acquisition of signals in the spectral domain. Fluorescence LIDAR with imaging capabilities has been developed in the field of cultural heritage studies to monitor the distribution of fluorescence features over a monument surface [24,25] or artworks [26]. The LIDAR imaging capabilities has been also used to monitor the stress status of a vegetation canopy [27].

The purpose of the present paper is to describe a new Hyperspectral Time-resolved Fluorescence LIDAR (HyT-FLIDAR) sensor, its operating principle and to show its capabilities in laser induced florescence map acquisition by raster scanning.

The hyperspectral time-resolved laser induced fluorescence spectra can be used both to apply temporal or spectral resolved data analysis techniques separately and to merge their capabilities. This synergy permits to obtain more detailed information on the different spectral contributions of targets showing a complex fluorescence behavior with respect to the temporal or spectral analysis alone. The hyperspectral and temporal resolution can also be used to apply fluorescence spectroscopy to volume fluorescent and/or attenuating media (such as water columns). The mapping capabilities of the system permit to extend these results to the monitoring of the surface/volume distribution of the fluorescence characteristics of the target.

## 2. Hyperspectral Time-resolved Fluorescence LIDAR (HyT-FLIDAR) sensor

The new LIDAR sensor with spectral and time resolution capabilities presented in this paper has been developed on the basis of a previous fluorescence imaging LIDAR system for the control of indoor and outdoor cultural heritage [28]. The most significant upgrades concern the implementation of a laser beam conditioning optical system, the development of the electronics for the accurate synchronization between laser and optical detector and the upgrade of the system control software.

Figure 1 shows a layout of the HyT-FLIDAR prototype. The excitation is provided by a tripled Nd:YAG (emitting at 355 nm) pulsed laser source (Continuum Minilite II) with a 5 ns pulse width, pulse energy of 8 mJ, beam diameter of 3 mm and a maximum repetition rate of 15 Hz. Beam conditioning optics (3X beam expander) have been implemented to reduce the laser divergence to about 1 mrad (full angle) in order to match the field of view of the collecting telescope. A couple of dichroic optics are used to steer the tripled Nd:YAG beam and to suppress the residual fundamental and doubled frequency components. The second steering optic aligns the excitation beam with the optical axis of the reflection telescope.

#184545 - $15.00 USD Received 14 Feb 2013; revised 10 May 2013; accepted 10 May 2013; published 13 Jun 2013

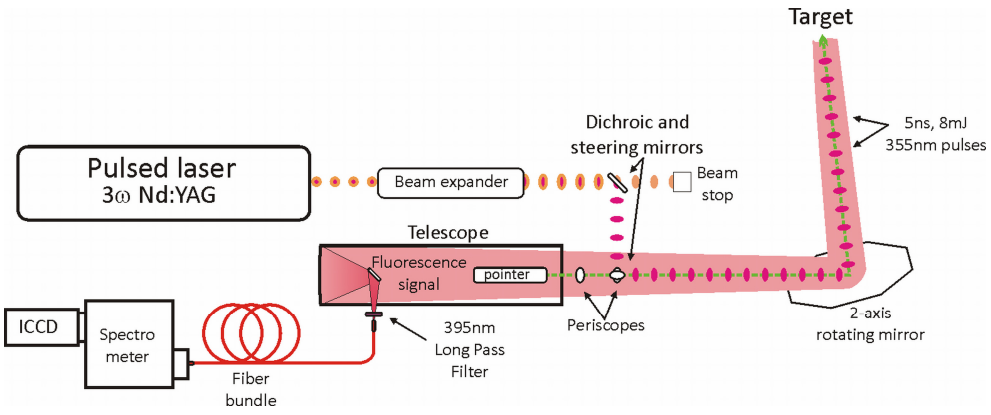


Fig. 1. Scheme of the HyT-FLIDAR.

The beam is sent to the pointing and scanning system used to point the laser beam to the target and to redirect the incoming light to the telescope. This is obtained by a movable folding mirror (640 mm x 260 mm) placed between the telescope and the target. A motorized mount permits the rotation of the steering mirror around two orthogonal axes (azimuthal and polar with respect to the telescope optical axis) with a rotation accuracy of about 0.2 mrad.

An additional laser source in the visible permits to point the target and to reference the fluorescence image. This laser emits few mW CW at 532 nm (class IIIa) with a divergence of 1.2 mrad. Its beam is made coaxial with the telescope optical axis. The nominal ocular hazard distance for both the CW reference laser at 532 nm and the UV pulsed laser at 355 nm (considering also the effect of the beam expander and the laser pulse energy actually sent to the target), operating separately, is about 12 m.

The light collected by the telescope (Newtonian, 1000 mm focal length, *f*/4) is filtered by a 395 nm long-pass volume absorption optical filter (Schott GG395) and then focused on a fiber optic bundle. The optical filter has the twofold function of rejecting the 355 nm backscattered radiation and of substantially avoiding higher spectral order contributions to the measured spectra. The entrance of the fiber optic bundle (50 silica fibers, 0.22 numerical aperture, 100 µm core diameter, 120 µm cladding diameter, disposed in a circular pattern) has a diameter of 1 mm. The fiber bundle entrance is moveable along the optical axis of the telescope so that it can be placed in the image plane corresponding to the target object plane, for target ranges between 4 m and infinity. The light collection efficiency of the telescope is optimized in this distance range. The output end of the bundle is placed as close as possible to the input slit of a flat field single spectrometer. At the output end of the bundle the fibers are disposed in a linear array matching the slit aperture in order to optimize the collection efficiency. The spectrometer is a PI-Acton SpectraPro 2300i with a focal length of 300 mm, *f*/3.9. The numerical aperture of the fiber bundle doesn't match the spectrometer *f*/#. This limitation in the coupling efficiency could be overcome by the use of optical fibers with reduced numerical aperture. The spectrometer is equipped with a computer-controlled motorized turret with three dispersion gratings (150 gg/mm, 600 gg/mm, 2400 gg/mm). A PI-Acton PI-Max:512 camera (ICCD, Intensified gated CCD, GEN-III intensifier, 512 X 512 pixels, pixel size 24 µm) was placed at the focal plane of the spectrometer.

The hyper-spectral time-resolved fluorescence LIDAR sensor has been equipped with an electronic board to synchronize the laser pulse with the ICCD gate. Kept constant the gate width, the opening time is sequentially delayed over different laser shots to acquire the backscattered light coming from the target with temporal resolution. The board, in-house developed using an Arduino Uno (by Arduino©) open-source single-board microcontroller platform, is the master-clock for the spectra acquisition procedure. The HyT-FLIDAR sensor is controlled by a computer equipped with an in-house developed software.

#184545 - $15.00 USD Received 14 Feb 2013; revised 10 May 2013; accepted 10 May 2013; published 13 Jun 2013

Figure 2 shows the acquisition procedure. The electronic board drives three independent TTL trigger signals: to the laser flash lamp (FL-Trig.), to the laser Q-switch (QS-Trig.) and to the camera external trigger input (C-Trig.). The delay (Ta) between the FL-Trig. and the QS-Trig. allows to set the laser pulse energy that reaches the maximum for a delay of about 150 μs. The QS-Trig. triggers the laser pulse that is emitted after some tens of nanoseconds and with a jitter of about 0.5 ns. Simultaneously to the QS-Trig., the C-Trig. triggers the camera onboard acquisition procedure. The delay (Tb) to the opening of the ICCD gate is controlled by the camera onboard circuitry and is selectable in the 25 ns to 20 ms range with a precision and accuracy of about 40 ps. The minimum gate width is 5 ns. The total jitter between the laser pulse emission and the ICCD gate is less than one nanosecond and permits to precisely synchronize the camera gate with the backscattering signal induced by the laser on the target. The spectrum collected by the ICCD is then transferred to the PC memory. It must be noticed that this acquisition also contains the ambient light background signal. After a time interval (Tc) of about 30 ms an additional C-Trig. is fired to acquire only the ambient light background in a separate acquisition. The backscattering signal induced by the laser is then obtained by subtraction. The gate widths used in the measurements and the wide dynamic range of the detector allow to operate the HyT-FLIDAR in full daylight. The acquisition sequence can be repeated and averaged over a selectable number of laser shots to increase the signal to noise ratio (SNR). Since the HyT-FLIDAR sensor is actually shot-noise limited, the SNR is proportional to the square root of fluorescence efficiency of the target and inversely proportional to the target distance in the far field (i.e. a distance longer than about 7 m).

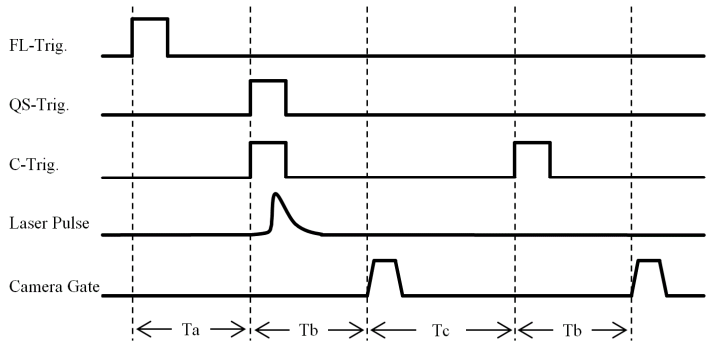


Fig. 2. Timing diagram of the acquisition procedure for a single fluorescence spectra.

As shown in Fig. 3, the spectrally and temporally resolved fluorescence measure is obtained as a series of several fluorescence spectra acquired with different Tb delay times (Tb1, Tb2 …). The gate width is usually kept constant within the series, typically at the minimum allowed by the camera (5 ns).

#184545 - $15.00 USD Received 14 Feb 2013; revised 10 May 2013; accepted 10 May 2013; published 13 Jun 2013

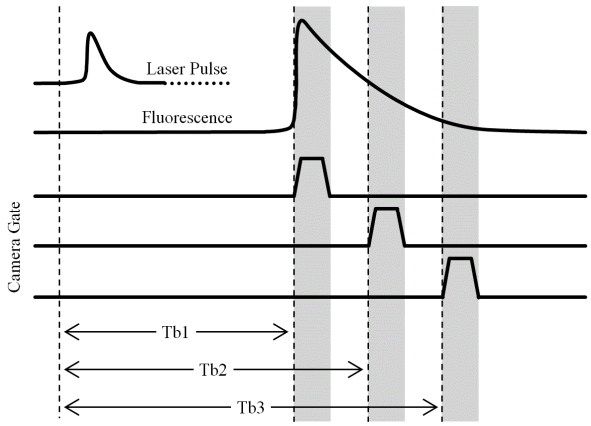


Fig. 3. Timing diagram of the temporal resolved acquisition procedure.

Figure 4 shows the temporal impulse response of the HyT-LIDAR sensor. The temporal impulse response was measured at 355 nm as the elastic backscatter signal from a highly reflecting metal target having a very low fluorescence emission. The measurement set-up, including target distance, and measurement protocol are the same used for the fluorescence measurements. The Tb delay times range has been set manually to cover the full duration of the backscattered signal. In this paper the initial delay time Tb1 has been chosen as the origin of temporal axes. The measured impulsive temporal response accounts for the temporal shape of the laser pulse, for the effective gate width and shape and for the jitters and it shows the possibility to achieve nanosecond time resolution and even sub-nanosecond time resolution by means of deconvolution of the time response itself.

For each delay value in the series the full spectrum in the range 350 nm – 810 nm is obtained by joining two different partially overlapped measurement in the windows 350 nm - 610 nm and 550 nm - 810 nm. The two spectral ranges are set by the PC using the 150 gg/mm dispersion grating. The pointing and scanning capabilities of the system permit to collect hyper-spectral, time-resolved fluorescence maps of the target by means of raster scanning of the target area under investigation. Table 1 summarizes the main features of the new LIDAR sensor.

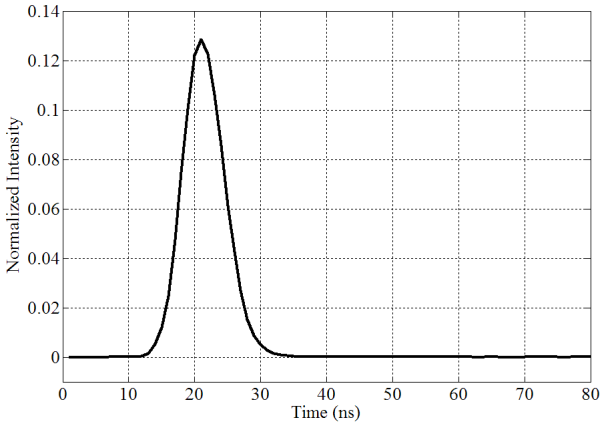


Fig. 4. Temporal impulse response of the sensor (intensity normalized at unitary integral).

#184545 - $15.00 USD Received 14 Feb 2013; revised 10 May 2013; accepted 10 May 2013; published 13 Jun 2013

**Table 1. HyT-FLIDAR main features.**

| Feature | Description |
|---|---|
| Excitation laser source | 3ω Nd:YAG, Q-Switched (@355 nm) 8 mJ @15 Hz, pulse width 5 ns |
| Optical reference system laser source | CW Laser @532 nm, <5 mW (class IIIa) |
| Detector | Intensified CCD 512 pixel × 512 pixel<br>QE>10% (in 150 nm - 870 nm range), Minimum gate width 5 ns |
| Spectrometer | 300 mm focal length, *f*/3.9, three dispersion gratings |
| Spectrometric linear resolution (spectral coverage) @435.8 nm | 150 gg/mm grating: 0.51 nm/pixel (260 nm)<br>600 gg/mm grating: 0.12 nm/pixel (63 nm)<br>2400 gg/mm grating: 0.02 nm/pixel (12 nm) |
| Telescope | Newtonian, 1000 mm focal length, *f*/4 |
| Operative distance range | 4 m up to infinity |
| IFOV | 1 mrad |
| Pointing system | Two axis motorized folding mirror |
| LIDAR Sensor Pointing field of view | Primary Axis: –30° up to + 210° from the reference direction<br>Secondary Axis: ± 45° from the orthogonal direction to telescope axis |
| Pointing accuracy (both axes) | 0.2 mrad |
| Weight and dimension | Size: 250 cm × 85 cm × 75 cm (l × h × w), Weight: about 150 kg |

## 3. Hyper-spectral time-resolved fluorescence spectra measurements

To illustrate the capabilities of the hyper-spectral time-resolved fluorescence LIDAR sensor, the measurements carried out on two different samples are shown. The two samples were a 150 mm x 174 mm Botticino sandstone slab (sample #1) and a 178 mm x 170 mm G10 epoxy fiberglass slab (sample #2).

More in details, Botticino is a red algae and bryozoan rudstone in a bioclastic packstone matrix. It is composed almost completely by $CaCO_3$ (Calcite) with traces of $SiO_2$ (quartz) [29]. Pure $CaCO_3$ and $SiO_2$ do not fluoresce under excitation at 355 nm: the sample fluorescence is almost completely due to its organic fraction [30], so that different fluorophores can coexist and can be observed in the sample, due to the various biological materials that contributed to the formation of the sandstone.

On the other hand, sample #2 is a man-made material: G10 is fabricated by embedding fiberglass in an epoxy resin obtained by polymerization of bisphenol A using aromatic amines as the hardener. Fluorescence in this material is due to its main constituents: Bisphenol A has a strong fluorescence peaked in the UV, whose tail extends down to 500 nm. Amines used for the curing also contribute to the fluorescence with broad bands in the visible [31,32]. For commercial reasons, dyes are often added to the material, which can contribute to its fluorescence.

These two samples have been chosen because of a high fluorescence efficiency, a rich and varied fluorescence spectral and temporal features and different fluorescence features homogeneity over each sample surface. Due to their similar fluorescence efficiency and decay time, these two samples can be measured efficiently using the same experimental setup and parameters. The measurements were carried out placing the samples at about 10 m from the LIDAR system. At this distance the diameter of the observed area is about 10 mm, corresponding to the target area reimaged on the fiber bundle entrance aperture.

In Fig. 5 the laser induced fluorescence backscattered signal intensity is reported in natural logarithmic scale as a function of wavelength and time in the spectral range between 350 nm and 810 nm and for a time interval of 200 ns. The time interval has been covered by changing the delay with 1 ns steps and keeping fixed the gate width at 5 ns. For each delay, 10 laser pulses have been averaged so that the acquisition time is about 4.5 minutes at the repetition rate of 15 Hz.

#184545 - $15.00 USD Received 14 Feb 2013; revised 10 May 2013; accepted 10 May 2013; published 13 Jun 2013

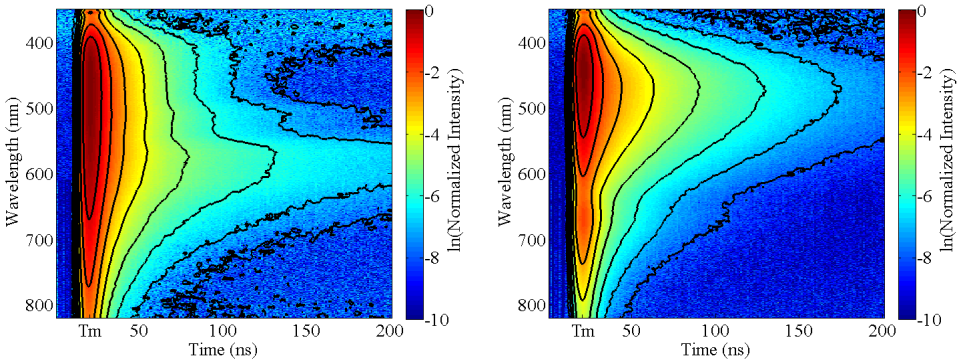


Fig. 5. Time –Wavelength, false color, intensity distribution of the acquired optical signal for sample #1 (left side) and sample #2 (right side). The intensity scale is natural logarithmic and normalized for each sample to the maximum of the entire data set. The time Tm corresponds to the maximum of the measured temporal impulse response of the sensor.

The analysis of acquired data allows extraction of information contained in both the spectral and the time domains. In Fig. 6 the time resolved spectra are reported for the two samples. The time resolved spectra show the signal at three different delay times corresponding to about 1, $e^{-2}$ and $e^{-4}$ times of the maximum intensity. In Fig. 6 the signal averaged over the whole 200 ns time interval (intensity normalized at unitary integral), is also reported. These spectra permit comparison of different fluorescence spectral and temporal behavior of the two samples and within each sample the different temporal evolution of the spectral distribution.

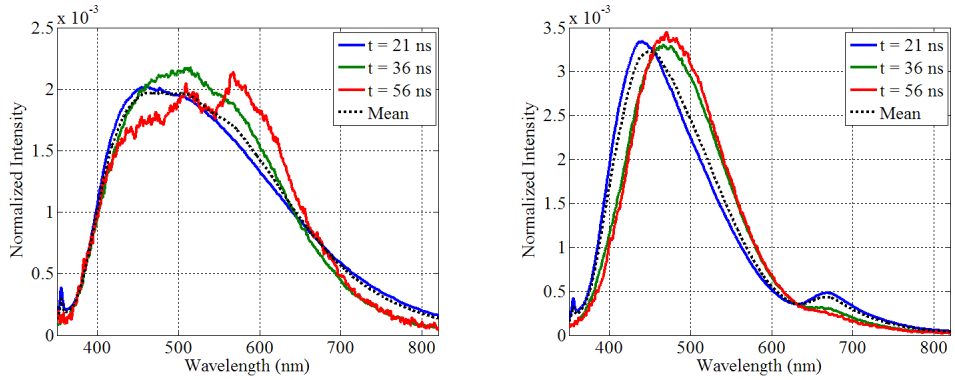


Fig. 6. Time resolved (solid line) and time averaged (dot line) spectra for samples #1 and #2, left and right side respectively. The time resolved spectra have been acquired at the indicated delays. Spectra are intensity normalized at unitary integral.

The variation of the fluorescence spectrum versus time as well as the dependence of the decay behavior over the emission wavelength is an indication of the presence of different fluorophores (e.g. bisphenol A and curing amines for the epoxy glass, different organic compounds embedded in the mineral matrix for the natural sandstone). Moreover, the temporal dependence of the decay time can be studied in order to understand the relaxation processes of the different fluorophores, and the possible occurrence of excitation transfer effects among different fluorophores.

In Fig. 7 we report the time-wavelength intensity distribution in natural logarithmic scale, normalized to the maximum occurring at each wavelength. The different shapes of the iso-intensity curves for the two samples give an instant look on the different contributions to the overall fluorescent emission.

#184545 - $15.00 USD Received 14 Feb 2013; revised 10 May 2013; accepted 10 May 2013; published 13 Jun 2013

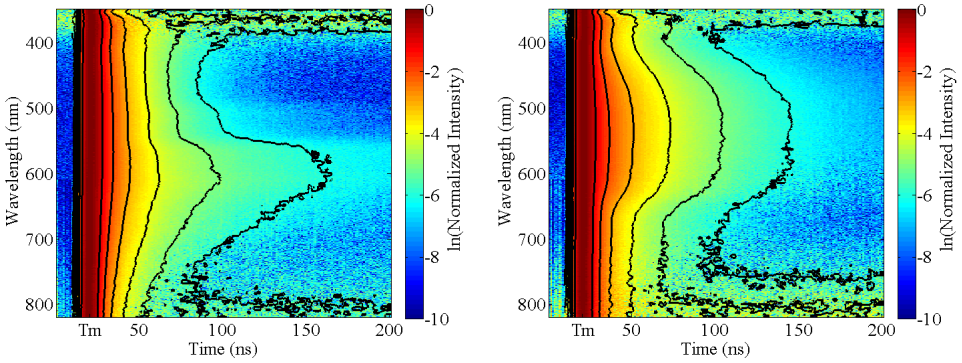


Fig. 7. Fluorescence time-wavelength intensity distribution normalized at the maximum at each acquisition wavelength. The time Tm corresponds to the maximum of the measured temporal impulse response of the sensor.

Figure 8 shows the natural logarithm of the fluorescence intensity decay profiles averaged over two spectral windows, 40 nm wide and centered at 460 nm and 680 nm (respectively band #1 and band #2) for the two samples. The temporal impulse response of the set-up is also reported for comparison. The decays do not appear as mono-exponential, indicating the coexistence of the emission from different transitions having different decay time. The weak peak (about $3 \cdot 10^{-4}$ times the maximum) of the system temporal impulse response at about 50 ns is actual and it is due to a small post lasing effect related to the laser Q-switch operation [33]. This post pulse is not visible in Fig. 4 because of the linear scale.

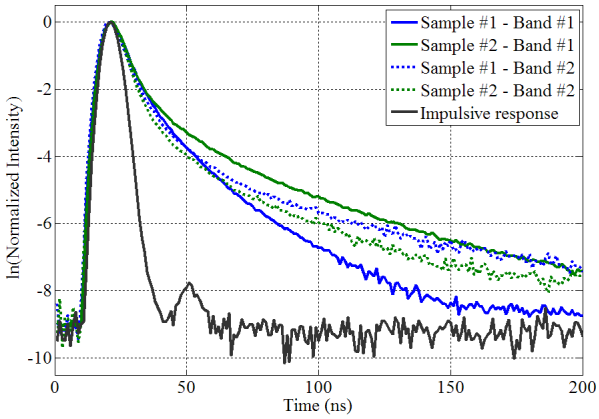


Fig. 8. Fluorescence intensity decay profiles at various acquisition wavelengths. Blue lines for sample #1 in band #1 (solid) and band #2 (dashed). Green lines for sample #2 in band #1 (solid) and band #2 (dashed). Black solid line for the system temporal impulse response for comparison. The plot reports the natural logarithm of data normalized to their maximum.

## 4. Hyper-spectral time-resolved fluorescence maps measurements

To enlighten the mapping capabilities of the Hyt-FLIDAR a target composed by the two samples described above was arranged as shown in Fig. 9, and placed at a distance of about 10 m. At this distance the single point measured area diameter is about 10 mm. The target was mapped with a 21 x 11 points rectangular grid, corresponding to an area of about 420 mm x 220 mm (sampling resolution 20 mm x 20 mm). Each point was measured in the spectral range between 350 nm and 810 nm and for a time interval of 80 ns (1 ns delay steps, gate width 5 ns, average of 4 laser pulses per delay step).

#184545 - $15.00 USD Received 14 Feb 2013; revised 10 May 2013; accepted 10 May 2013; published 13 Jun 2013

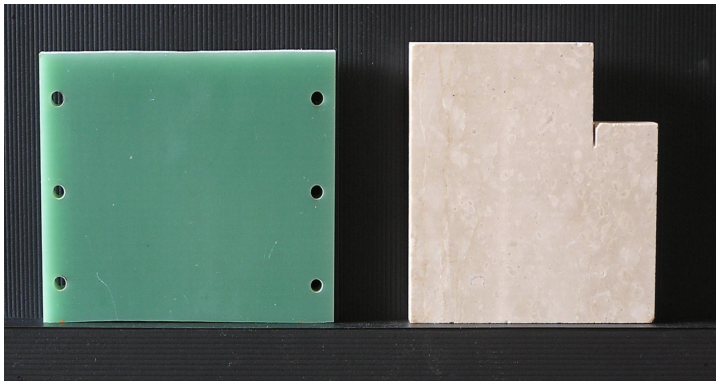

Fig. 9. Composite target used to test the LIDAR mapping capabilities, constituted by the G10 epoxy fiberglass slab (left side) and the Botticino sandstone slab (right side). The background is a black polymer screen.

Figure 10 shows the spatial distribution of the ratio between the fluorescence intensity in the spectral bands #1 and #2 described above. The fluorescence intensity was previously averaged over the whole measured time interval (80 ns). The ratio value corresponding to the black background was set to zero, due to the high noise caused by the low level of signal.

Figure 11 shows the results of data processing in the temporal domain performed by the study of the decay behavior of the fluorescence intensity in the band #1. For each pixel we report the time delay between the signal maximum and its reduction to $e^{-4}$ value. The time delay values have been evaluated with a precision better than the time sampling delays by applying a smoothing cubic spline procedure [34]. The time constant for the background is set to zero.

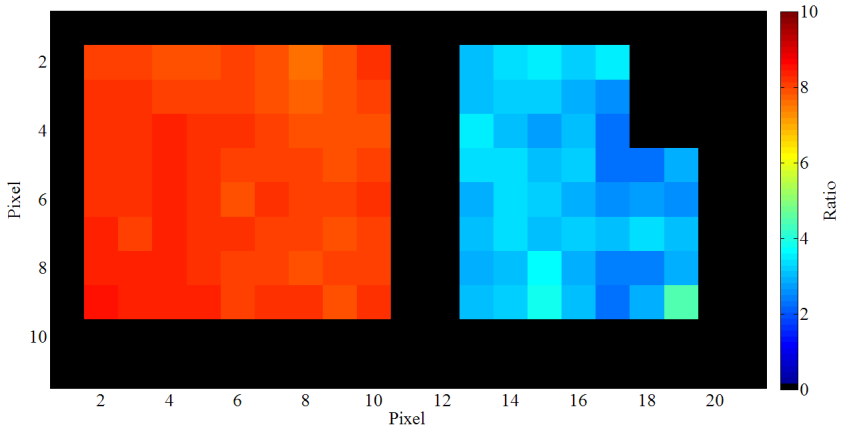


Fig. 10. Spatial distribution of the ratio between the fluorescence intensity in the spectral bands #1 and #2. The fluorescence intensity was previously averaged over the full 80 ns measured time lapse. The ratio value corresponding to the black background was set to zero. Ratio for the G10 epoxy fiberglass slab and the Botticino sandstone slab are, respectively, 8.1 ± 0.2 and 3.0 ± 0.4 (mean ± std).

#184545 - $15.00 USD Received 14 Feb 2013; revised 10 May 2013; accepted 10 May 2013; published 13 Jun 2013

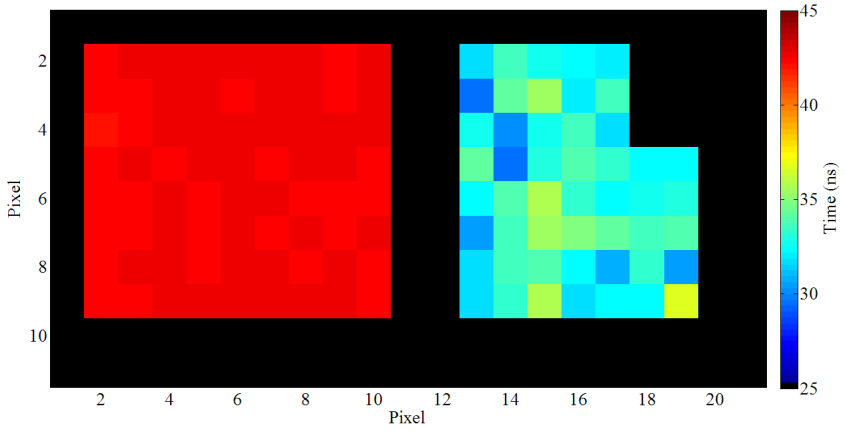


Fig. 11. Spatial distribution of the time needed to reach $e^{-4}$ of the maximum of fluorescence in the spectral band #1. The time constant for the background is set to zero. Time delays for the G10 epoxy fiberglass slab and the Botticino sandstone slab are, respectively, 42.5 ± 0.2 ns and 32.8 ± 1.6 ns (mean ± std).

The G-10 epoxy glass sample shows a remarkable uniformity across its whole extension of the fluorescence spectral shape and temporal behavior: this is not surprising, considering that this is a material having a uniform composition and structure. Conversely, Botticino sandstone shows a significant variation both in the spectral shapes and in the fluorescence decay times across its extension. This is due to the non-uniform distribution of the different fluorophores across the sample, resulting from the natural formation process. Actually, local variations in the composition and in the chromophores content of the sample are also evident by visual inspection, as a variation in the color shade of the surface (see Fig. 9).

It can be seen that this analysis can provide important information for the identification of the sample constituents. The whole data set can be usefully analyzed both for the study of the chemical properties of the constituent of an unknown sample and for the identification and mapping of a known constituent in a structured sample.

## 5. Conclusion

We have presented the new Hyperspectral Time-resolved Fluorescence LIDAR (HyT-FLIDAR) that is capable to acquire a hyperspectral time resolved 4-D hypercube of the fluorescence intensity emitted by the excited sample. The set-up can provide nanosecond time resolution, a better than one nanometer spectral resolution and a sub-milliradiant angular mapping resolution. The HyT-FLIDAR prototype capabilities have been illustrated by the single spectra and mapping measurement of extended and composite targets. The acquired data have been analyzed in order to extract from the fluorescence spectral and/or temporal behavior information about the presence of different fluorophores, their relaxation processes and the occurrence of excitation transfer effects among them. The possibility to acquire a 2-D maps of this datum provides a very versatile tool for the identification of inhomogeneities of an extended target, particularly interesting in artwork, environmental and geological applications.

#184545 - $15.00 USD Received 14 Feb 2013; revised 10 May 2013; accepted 10 May 2013; published 13 Jun 2013